Journal of Water Process Engineering 48 (2022) 102936

Contents lists available at ScienceDirect

Journal of Water Process Engineering

journal homepage: www.elsevier.com/locate/jwpe

Inactivation of plant pathogenic bacterium *Ralstonia solanacearum* in drainage solution from hydroponic system by a rotating advanced oxidation contactor equipped with TiO_2/zeolite composite sheets

Youhei Nomura [a,b,*], Koutaro Koga [c], Kouhei Ohnishi [d], Shuji Fukahori [e], Taku Fujiwara [a,b,f]

[a] Research and Education Faculty, Natural Sciences Cluster, Agriculture Unit, Kochi University, 200 Monobe, Otsu, Nankoku, Kochi 783-8502, Japan
[b] Department of Environmental Engineering, Graduate School of Engineering, Kyoto University, C1-2, Kyoto-Daigaku-Katsura, Nishikyo-ku, Kyoto 615-8540, Japan
[c] Faculty of Agriculture and Marine Science, Kochi University, 200 Monobe, Otsu, Nankoku, Kochi 783-8502, Japan
[d] Research Institute of Molecular Genetics, Kochi University, 200 Monobe, Otsu, Nankoku, Kochi 783-8502, Japan
[e] Paper Industry Innovation Center of Ehime University, 127 Mendori-cho, Shikokuchuo, Ehime 799-0113, Japan
[f] IoP Collaborative Creation Center, Kochi University, 200 Monobe, Otsu, Nankoku, Kochi 783-8502, Japan

ARTICLE INFO

Keywords:
Rotating advanced oxidation contactor
TiO_2/zeolite composite sheet
Ralstonia solanacearum
Inactivation
Hydroponic system
Drainage solution

ABSTRACT

A rotating advanced oxidation contactor (RAOC) equipped with TiO_2/zeolite composite sheets was developed to inactivate the plant pathogenic bacterium *Ralstonia solanacearum* in drainage solution (DS) from a hydroponic system. The inactivation efficiency of *R. solanacearum* in DS and pure culture solution (PS) by the RAOC was compared with that achieved by a submerged composite sheet photocatalysis reactor (SSPR). The initial number of living bacteria (N_0) was adjusted to around 10^6–10^7 CFU mL^{-1}. The inactivation efficiency of *R. solanacearum* by the SSPR at 4.0×10^7 CFU mL^{-1} of N_0 significantly decreased compared with that at 1.8×10^6 CFU mL^{-1} of N_0 owing to the attenuation of UV intensity by light absorption and scattering by solids derived from *R. solanacearum*, while the RAOC achieved >2-log inactivation during 24 h of treatment regardless of N_0. The inactivation of *R. solanacearum* by the RAOC decelerated after 6 h, possibly because of competition for reactive oxygen species between *R. solanacearum* and products accumulated by inactivation of *R. solanacearum*. The ratio of rate constants for inactivation of *R. solanacearum* in DS to that in PS by the RAOC was 8 times that for the SSPR. This shows that the RAOC greatly mitigates the light attenuation and inhibitory effects of coexisting substances on inactivation of *R. solanacearum* in the DS. The RAOC is therefore a promising and upscalable photocatalytic reactor for efficient inactivation of *R. solanacearum* in DS.

1. Introduction

The global population will rise from around 7 billion people in 2010 to nearly 10 billion by 2050 [1], and food production in 2050 will need to be increased by 56 % compared with that in 2010 [2]. Agriculture plays an essential role in food production. Soil culture has greatly contributed to vegetable production, but suffers problems such as excessive use of water [3,4], emission of greenhouse gases including nitrous oxide [5,6], and occurrence of soilborne diseases [7,8]. Thus, hydroponic culture—an approach for growing plants without soil that involves using nutrient solutions in water—has been used in farming as an alternative to soil culture. The closed hydroponic system enables one to save water and nutrients by cyclic use of the drainage solution (DS) and exhibits higher yield per unit area than soil culture [9–11]. Although the hydroponic system can avoid occurrence of soilborne diseases, plant pathogens can invade the system via various routes such as from the substrate, seeding, and soil surrounding the hydroponic greenhouse [12], resulting in significant decrease in crop yield.

Disinfection of the DS to inactivate plant pathogens (e.g., *Fusarium* spp.) has been explored by a wide variety of approaches such as heating [13], membrane filtration [14,15], chlorination [16], liming [17], ozonation [18], corona plasma [18–23], ultraviolet (UV) irradiation [24], and photocatalysis [25,26]. Heating and membrane filtration have limitations such as high running cost and a requirement for periodic cleaning maintenance. Although chlorination is cost-effective, continuous addition of chlorine may have an adverse impact on the plants such

* Corresponding author at: Department of Environmental Engineering, Graduate School of Engineering, Kyoto University, C1-2, Kyoto-Daigaku-Katsura, Nishikyo-ku, Kyoto 615-8540, Japan.
E-mail address: nomura.yohei.3r@kyoto-u.ac.jp (Y. Nomura).

https://doi.org/10.1016/j.jwpe.2022.102936
Received 12 March 2022; Received in revised form 6 May 2022; Accepted 8 June 2022
Available online 17 June 2022

as formation of chloramines, which have detrimental effects, via the reaction of ammonia and residual chlorine or sodium hypochlorite in the nutrient solution [16,27]. Ozonation and corona plasma generate highly reactive oxygen species (e.g., hydroxyl radicals), and a huge amount of electrical energy is required for the operation.

Inactivation of plant pathogens using UV irradiation and a photocatalyst such as titanium dioxide (TiO_2) has been reported [24–26,28,29]. Photocatalysts produce reactive oxygen species (e.g., hydroxyl radicals) under UV irradiation, and photocatalysis is expected to be an energy-saving advanced oxidation process (AOP) because sunlight can be used as the light source. However, the efficiency of inactivating pathogens by UV-based AOPs including photocatalysis decreases with increasing reactor volume because of scattering and attenuation of light in water [28,29].

Economic losses due to bacterial wilt disease, which is caused by the soilborne plant pathogenic bacterium *Ralstonia solanacearum*, are a growing agricultural concern worldwide. Infection of hydroponically-cultivated tomato (*Solanum lycopersicum*) by *R. solanacearum* has been reported [30]. *R. solanacearum* infects into plant root and colonizes the intercellular spaces of the root. Subsequently, *R. solanacearum* invades xylem vessels and reduces sap flow by growth of bacterial cells and formation of exopolysaccharide slime, resulting in the development of wilting symptoms [31,32]. In closed hydroponic systems, *R. solanacearum* is diffused throughout the cultivation facility in the recirculating DS, and eradicating *R. solanacearum* is very difficult after the appearance of symptoms. Hence, development of disinfection techniques for DS containing *R. solanacearum* is urgently required. Corona plasma is the only technology that has been applied for *R. solanacearum* inactivation, and the corona discharge reactor showed good performance in repetitively and continuously inactivating *R. solanacearum* in artificial nutrient solution [19–21,23]. However, previous studies have not assessed the inactivation of *R. solanacearum* in an actual DS, and have not considered the inhibitory effects of coexisting substances in the DS on the inactivation efficiency. We previously investigated the DS water quality from hydroponic system and revealed that DS contains a wide variety of coexisting substances at high concentration [33]. Evaluating the inactivation efficiency in actual DS instead of artificial nutrient solution is also important because some of organic compounds such as carboxylates exhibit a lower reactivity with hydroxyl radicals [34,35]. In addition, the corona discharge reactor requires continuous air flow as well as high voltage to produce reactive oxygen species and is hard to scale-up. From an engineering viewpoint, the development of an upscalable reactor for inactivating *R. solanacearum* in DS is of great importance.

We have fabricated a composite sheet with TiO_2 and adsorbent (e.g., zeolite) using a papermaking technique to easily separate the functional materials from treated water [36,37], and developed a rotating advanced oxidation contactor (RAOC) equipped with the TiO_2/zeolite composite sheets [38,39]. In the RAOC, the top part of the disk is illuminated with UV light for photocatalysis, and the bottom part of the disk is immersed in water for adsorption of organic contaminants. By rotating the disk, the photocatalysis and adsorption occur continuously. The RAOC shows excellent performance for removing trace organic contaminants from actual wastewater and greatly mitigates the inhibitory effects of coexisting substances in addition to light attenuation as the photocatalysis is performed in an extremely thin water film [40,41]. We have found that water temperature and UV intensity are key factors for controlling the performance of RAOC treatment [41,42], and this technology is expected to be cost-effective and energy-saving for treatment of organic contaminants in reverse osmosis concentrate from water reuse [43,44]. The RAOC is an upscalable reactor and applicable to actual wastewater treatment systems to remove trace organic contaminants. However, no previous research has applied the RAOC to disinfection of DS infested by *R. solanacearum*.

In this study, the efficiency of inactivation of *R. solanacearum* by an RAOC equipped with TiO_2/zeolite composite sheets was evaluated in comparison with that by a submerged composite sheet photocatalysis reactor (SSPR). In addition, fluorescent protein-labelled *R. solanacearum* was used to estimate the material that captures and inactivates the *R. solanacearum* in the TiO_2/zeolite composite sheet. The inhibitory effects of coexisting substances in the DS on inactivation of *R. solanacearum* were investigated by comparing the inactivation efficiencies in pure culture solution (PS) and DS. To the best of our knowledge, this is the first report of development of an upscalable photocatalytic reactor to inactivate *R. solanacearum* in DS.

2. Materials and methods

2.1. Materials

The sources of chemicals are provided in Appendix A Text S1. *R. solanacearum* strain OE1–1 [45] was selected as the target strain in this study and was incubated in B medium [46] by shaking at 28 °C for 24 h to reach stationary phase [nearly 10^9 colony-forming units (CFU) mL^{-1}]. To visualize the distribution of *R. solanacearum* on the sheets, a green fluorescent protein (GFP)-labelled *R. solanacearum* strain OE1–1 (GFP-labelled *R. solanacearum*) [47] was used. The DS from a hydroponic system for eggplant cultivation (Kochi, Japan) was collected on December 18, 2019. The DS quality is summarized in Table 1. Electric conductivity and pH of the DS were measured immediately after sampling. The wide range of electric conductivity value was observed (20–472 mS m^{-1}) in our previous study [33], and the value measured in present study was within the range. Suspended solids concentration in the DS was below the detection limit, and the DS was stored at 4 °C after filtration with glass fiber filtration papers (Whatman GF/B, Pittsburg, PA, USA). Because the DS might contain bacteria in addition to *R. solanacearum*, the DS was sterilized at 121 °C for 30 min using a high-pressure steam sterilizer (MLS-3030, PHC Holdings Corporation, Tokyo, Japan) before conducting disinfection experiments, and *R. solanacearum* cells were added to the sterilized DS. The DS water quality before and after sterilization is shown in Appendix A Table S1.

2.2. Configuration of reactors

The polyethylene terephthalate (PET) fiber, zeolite, TiO_2, and TiO_2/zeolite containing sheets were prepared using a dual polymer retention system. PET fiber sheet (containing 6.25 g of PET fibers), zeolite sheet (containing 6.25 g of PET fibers and 3.125 g of zeolite), TiO_2 sheet (containing 6.25 g of PET fibers and 3.125 g of TiO_2), and TiO_2/zeolite composite sheet (containing 6.25 g of PET fibers, 3.125 g of zeolite, and 3.125 g of TiO_2) were obtained. The details of preparation and physiochemical properties of the TiO_2/zeolite composite sheet are shown in our previous study [37]. We previously confirmed that TiO_2 and zeolite particles were uniformly dispersed within TiO_2/zeolite composite sheet, and the composite sheet has high durability toward UV irradiation [37].

Table 1
DS water quality.

Index	Unit	Value
pH	–	6.2
EC	mS m^{-1}	26.4
M-alkalinity	mg $CaCO_3$ L^{-1}	23.5
DOC	mg C L^{-1}	9.33
Absorbance at 365 nm	cm^{-1}	0.10
Na^+	mg L^{-1}	19.6
NH_4^+	mg L^{-1}	2.02
K^+	mg L^{-1}	431
Mg^{2+}	mg L^{-1}	91.6
Ca^{2+}	mg L^{-1}	109
Cl^-	mg L^{-1}	1.48
NO_3^-	mg L^{-1}	1060
SO_4^{2-}	mg L^{-1}	233
PO_4^{3-}	mg L^{-1}	224

In the present study, the SSPR and RAOC were configured as shown in Fig. 1. In the SSPR, the TiO_2/zeolite composite sheet with effective area of 9 cm^2 (1.8 cm × 5 cm) was completely immersed in a glass vial filled with test culture solution (0.05 L), and the vial was illuminated with a UVA light source (λ = 350–400 nm, maximum wavelength 365 nm, FL287-BL365, Raytronics Corporation, Saitama, Japan). A UVA light source was chosen because solar light is expected to be used in future applications. In the RAOC, two pieces of TiO_2/zeolite composite sheet with an effective area of 449 cm^2 for each piece were fixed (one on each side) on a disk with diameter of 24 cm. The bottom part of the disk (45 % of the disk area) was submerged in a tank (25 cm × 7 cm × 14.5 cm) filled with test culture solution (2 L) for adsorption, and the top part of the disk (55 % of the disk area) was illuminated with the UVA light source (FL287-BL365) to achieve photocatalysis. The rotation speed of the disk was controlled at 10 rpm by a motor. A UV radiometer (UV-340C, Custom Corporation, Tokyo, Japan) was used to measure the UV intensity at the surface of the vial or disk.

2.3. Inactivation of *R. solanacearum*

Cultures of *R. solanacearum* for inactivation were prepared by diluting the bacterial cells using PS or DS, and the number of initial living bacteria (N_0) was adjusted to around 10^6–10^7 CFU mL^{-1}. In this study, 10 mM $MgSO_4$ was used as the PS. Inactivation tests of *R. solanacearum* were performed using the SSPR or RAOC. The experimental conditions are summarized in Table 2. *R. solanacearum* was used in RUNs X1–X7, and GFP-labelled *R. solanacearum* was used in RUNs Y1–Y5. RUNs X1 and Y1–Y4 were conducted in dark, and RUNs X2–X7 were performed with UV illumination of 1 mW cm^{-2} (corresponding to a UV fluence rate of 3.6 × 10^3 mJ cm^{-2} h^{-1}). In RUN Y5, four pieces of sheet with an effective area of 224.5 cm^2 for each piece were fixed on a disk with a surface area of 898 cm^2, and the experiment was performed during 0–6 h in dark and 6–12 h with UV illumination of 1 mW cm^{-2}. The water temperature was adjusted to 25 ± 1 °C. At the designated time, 1 or 10 mL of treated solution was taken, and the number of living bacteria (N) and the UV spectrum were measured. The glassware and reactor were sterilized before conducting disinfection experiments. All tests were carried out twice.

2.4. Analytical methods

2.4.1. Quantitative methods

N_0 and N were measured using the dilution plate technique. The sample was diluted using 10 mM $MgSO_4$, and 100 μL of sample were spread on a plate containing BG medium [46]. To measure the N in the sheet, we referred the standard methods for DNA extraction [48]. The sheet sample (2 cm^2) immersed in the PS (1 mL) was vortexed for 5 s, and the N in the solution was measured. To selectively incubate *R. solanacearum*, the antibiotic polymyxin B sulfate was added to the BG medium [49]. The plate was incubated at 28 °C in the dark, and colonies were counted after 48 h [50]. A spectrophotometer (Biospec-1600, Shimadzu Corporation, Kyoto, Japan) was used with a quartz cell (light path length 1 cm) to measure absorbance at 660 nm (A_{660}), 365 nm (A_{365}), and 230 nm (A_{230}), and the initial values ($A_{0,660}$, $A_{0,365}$, and $A_{0,230}$) in RUNs X2–X5 are summarized in Table 2. The bacterial distribution on the sheets was observed using epifluorescence microscope (BX51, Olympus Optical Co., Tokyo, Japan). Analytical methods for dissolved organic carbon (DOC) and inorganic ions are given in Appendix A Text S2.

2.4.2. Kinetic analysis

Chick-Watson model [51,52] has been used for analyzing the inactivation kinetics of bacterial pathogens by photocatalysis [53,54]; thus, the model was used in this study. Chick-Watson equation is expressed as follows:

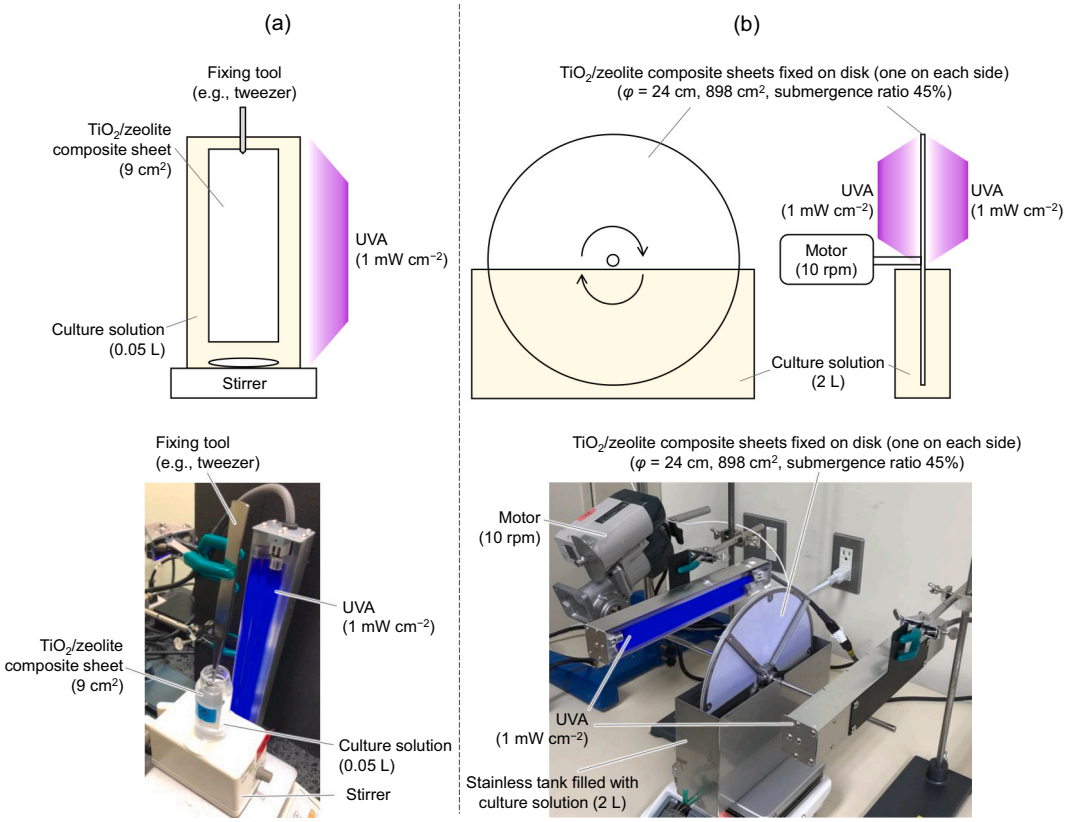

Fig. 1. Configuration of reactors. a. Submerged composite sheet photocatalysis reactor (SSPR); b. Rotating advanced oxidation contactor (RAOC).

Table 2
Experimental conditions.

RUN	Sheet*	Reactor	Target	Solvent	N_0 (CFU mL^{-1})	$A_{0,660}$ (−)	$A_{0,365}$ (−)	$A_{0,230}$ (−)	UV intensity (mW cm^{-2})
X1	TiO_2/zeolite	SSPR	*R. solanacearum*	PS	2.6×10^6	–	–	–	0 (dark)
X2	TiO_2/zeolite	SSPR	*R. solanacearum*	PS	1.8×10^6	0.004	0.013	0.076	1
X3	TiO_2/zeolite	SSPR	*R. solanacearum*	PS	4.0×10^7	0.023	0.084	0.504	1
X4	TiO_2/zeolite	RAOC	*R. solanacearum*	PS	3.0×10^6	0.002	0.009	0.055	1
X5	TiO_2/zeolite	RAOC	*R. solanacearum*	PS	3.0×10^7	0.021	0.088	0.498	1
X6	TiO_2/zeolite	SSPR	*R. solanacearum*	DS	2.9×10^6	–	–	–	1
X7	TiO_2/zeolite	RAOC	*R. solanacearum*	DS	2.5×10^6	–	–	–	1
Y1	PET	SSPR	GFP-labelled *R. solanacearum*	PS	1.9×10^6	–	–	–	0 (dark)
Y2	Zeolite	SSPR	GFP-labelled *R. solanacearum*	PS	1.9×10^6	–	–	–	0 (dark)
Y3	TiO_2	SSPR	GFP-labelled *R. solanacearum*	PS	1.9×10^6	–	–	–	0 (dark)
Y4	TiO_2/zeolite	SSPR	GFP-labelled *R. solanacearum*	PS	1.9×10^6	–	–	–	0 (dark)
Y5	PET Zeolite TiO_2 TiO_2/zeolite	RAOC	GFP-labelled *R. solanacearum*	PS	2.0×10^6	–	–	–	0 (0–6 h, dark) 1 (6–12 h)

PET: polyethylene terephthalate
SSPR: submerged composite sheet photocatalysis reactor
RAOC: rotating advanced oxidation contactor
GFP: green fluorescent protein
PS: pure culture solution
DS: drainage solution from a hydroponic system
N_0: the number of initial living bacteria
$A_{0,660}$, $A_{0,365}$, $A_{0,230}$: initial values of absorbance at 660 nm, 365 nm, and 230 nm.
* The PET fiber sheet, zeolite sheet, TiO_2 sheet, and TiO_2/zeolite composite sheet were used in this study. In RUN Y5, four pieces of sheet with an effective area of 224.5 cm^2 for each piece were fixed on a disk with a surface area of 898 cm^2.

$$\frac{dN}{dt} = -kN \quad (1)$$

where k is the rate constant for inactivating *R. solanacearum* (h^{-1}), and t is UV irradiation time (h). The definitions of N and N_0 are given above.

2.4.3. Statistical analysis

The effect of N_0 on *R. solanacearum* inactivation and the inhibition of inactivation of *R. solanacearum* by coexisting substances in DS were evaluated by statistically analyzing the rate constant for *R. solanacearum* inactivation. One-tailed t-test for equal variances was performed using Microsoft Excel Version 16.60. The significance level was set at p value$<$0.05.

3. Results and discussion

3.1. Inactivation of R. solanacearum in the PS by the SSPR

The inactivation behaviors of *R. solanacearum* in PS by the SSPR are shown in Fig. 2a (RUNs X1–X3). In RUN X1 (dark conditions), log (N/N_0) slightly decreased until 2 h through adsorption by the TiO_2/zeolite composite sheet and then gradually increased during 3–24 h by bacterial growth. In RUN X2 (with UV irradiation), log (N/N_0) continuously decreased, and nearly 2-log inactivation was achieved during 24 h of SSPR treatment. We confirmed that *R. solanacearum* continued to grow in the absence of the composite sheet and UV irradiation, and it was not inactivated by irradiation with the UVA light used in this study (Fig. S1). This shows that *R. solanacearum* is inactivated through photocatalysis by the TiO_2/zeolite composite sheet under UV irradiation. In RUN X3 (with UV irradiation), only 0.5-log reduction was observed during 24 h of SSPR treatment, and the inactivation efficiency of *R. solanacearum* in RUN X3 significantly decreased compared with that in RUN X2. Because a linear relationship was observed between ln (N/N_0) and time during 0–6 h, the k for inactivation of *R. solanacearum* were determined from the slopes of the regression lines during 0–6 h (Fig. S2). The k value in RUN X3 (k_{X3}, 3.20×10^{-2} h^{-1}) was an order of magnitude lower than that in RUN X2 (k_{X2}, 4.09×10^{-1} h^{-1}). The behaviors of GFP-labelled *R. solanacearum* in PS by the SSPR are shown in Fig. 3a (RUNs Y1–Y4). In RUNs Y1–Y4, log (N/N_0) did not change. The N in the sheet is shown in Fig. 4. In RUNs Y1–Y4, the living bacteria were detected from each sheet. This indicates that the GFP-labelled *R. solanacearum* was captured by the sheet. The fluorescence images of each sheet after 6 h of SSPR treatment are shown in Fig. 5. The PET fibers are narrow (Fig. 5a, b, c, and d), and flocs containing TiO_2 particles were observed inside the fiber network (Fig. 5c and d). Although flocs of zeolite particles could not be observed by fluorescence microscopy (Fig. 5b), we previously confirmed that particles of TiO_2 and zeolite are uniformly dispersed within the TiO_2/zeolite composite sheet by scanning electron microscopy/energy dispersive X-ray spectroscopy [37]. The GFP-labelled *R. solanacearum* was observed on PET fiber and the flocs of TiO_2 particles from all types of sheet (Fig. 5a, b, c, and d), and mainly observed on PET fibers. We deduce that PET fibers in the TiO_2/zeolite composite sheet play an important role in capturing *R. solanacearum*. Time profiles of A_{660} and A_{365} are shown in Fig. 6. A_{660} is used to evaluate the turbidity of water containing solids. The value of $A_{0,660}$ in RUN X3 was higher than that in RUN X2 as was N_0 (Table 2) because more solids derived from *R. solanacearum* were observed in RUN X3. A decrease in $A_{660}/A_{0,660}$ due to the SSPR treatment was confirmed in both RUN X2 and RUN X3 (Fig. 6a). During 24 h of SSPR treatment, $A_{660}/A_{0,660}$ reached zero in RUN X2, while it remained around 0.5 in RUN X3. A_{365} was also measured because a UVA light source, whose maximum wavelength was 365 nm, was used in this study. The values of $A_{365}/A_{0,365}$ at 24 h in RUN X2 and RUN X3 were 0.18 and 0.46, respectively (Fig. 6b). This indicates that UV-absorbing substances remained at a higher concentration in RUN X3 than in RUN X2 and the photon flux on the TiO_2 surface in RUN X3 was lower than that in RUN X2. Previous studies showed that solids strongly affect the photocatalytic performance of TiO_2 because of light scattering by the solids [55,56]. We

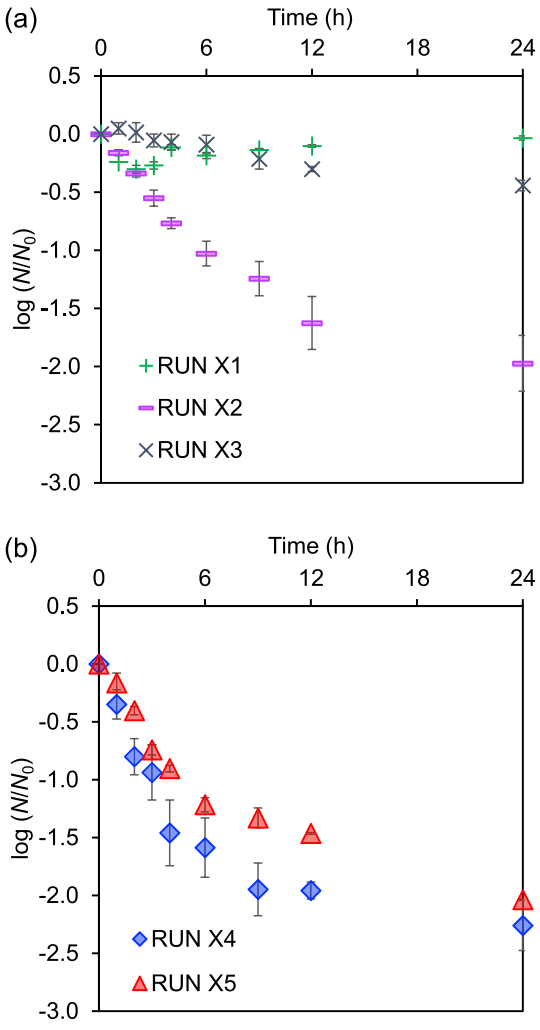

Fig. 2. Inactivation of *Ralstonia solanacearum* in pure culture solution (PS) by the SSPR (a, RUNs X1–X3) and the RAOC (b, RUNs X4 and X5). The N_0 in RUNs X1, X2, X3, X4, and X5 were 2.6×10^6, 1.8×10^6, 4.0×10^7, 3.0×10^6, and 3.0×10^7 CFU mL^{-1}, respectively. In RUNs X1–X5, the water temperature was adjusted at 25 ± 1 °C. RUN X1 was conducted in dark, and RUNs X2–X5 were performed with UV illumination of 1 mW cm^{-2}. The plots are the average of measured values, and error bars denote the range of measured values ($n = 2$).

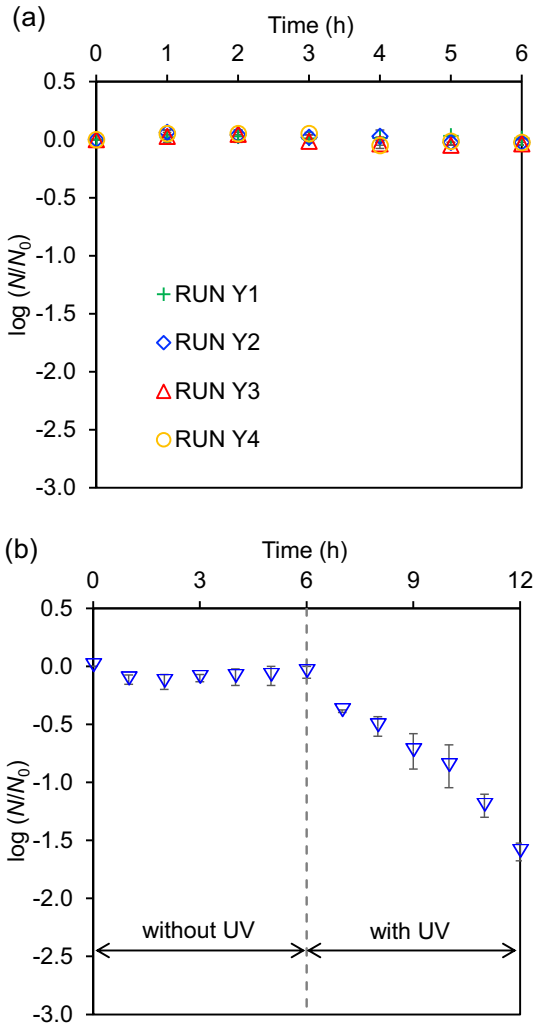

Fig. 3. Behaviors of GFP-labelled *R. solanacearum* in pure culture solution (PS) by the SSPR (a, RUNs Y1–Y4) and the RAOC (b, RUN Y5). The N_0 in RUNs Y1–Y4 and Y5 were 1.9×10^6 and 2.0×10^6 CFU mL^{-1}, respectively. In RUNs Y1–Y5, the water temperature was adjusted at 25 ± 1 °C. RUNs Y1–Y4 were conducted in dark. RUN Y5 was conducted during 0–6 h in dark and performed during 6–12 h with UV illumination of 1 mW cm^{-2}. The plots are the average of measured values, and error bars denote the range of measures values ($n = 2$).

deduce that the significant decrease in k value with increase in N_0 from 1.8×10^6 CFU mL^{-1} to 4.0×10^7 CFU mL^{-1} might be attributed to the attenuation of UV intensity by light absorption and scattering by solids derived from *R. solanacearum*.

3.2. Inactivation of *R. solanacearum* in PS by the RAOC

The inactivation behaviors of *R. solanacearum* in PS by the RAOC are shown in Fig. 2b (RUNs X4 and X5). The RAOC successfully inactivated *R. solanacearum* under UV irradiation, and >2-log inactivation was achieved during 24 h of RAOC treatment in both RUNs X4 and X5. The inactivation behavior in RUN X5 was similar to that in RUN X4, despite the presence of *R. solanacearum* at one order of magnitude higher N_0. In RUN Y5, log (N/N_0) was almost stable during 0–6 h and decreased during 6–12 h (Fig. 3b). As shown in Fig. 4, the N in the PET fiber sheet and zeolite sheet at 6 h was almost same with that at 12 h, while the N in the TiO_2 sheet and TiO_2/zeolite composite sheet at 12 h was significantly lower than that at 6 h. This shows that *R. solanacearum* is inactivated through TiO_2/UV photocatalysis. Therefore, *R. solanacearum* captured by the sheet is inactivated through photocatalysis by the TiO_2/zeolite composite sheet under UV irradiation. From the behavior of $A_{660}/A_{0,660}$ (Fig. 6a), the solids were completely removed during 24 h of RAOC treatment in both RUNs X4 and X5. The values of $A_{365}/A_{0,365}$ at 24 h in RUN X4 and RUN X5 were 0.17 and 0.05, respectively (Fig. 6b). This indicates that almost all UV-absorbing substances were removed during 24 h of RAOC treatment during 24 h of the RAOC treatment in both RUNs X4 and X5. Although the rate of inactivation of *R. solanacearum* by SSPR in RUN X3 significantly decreased compared with that in RUN X2 owing to the attenuation of UV intensity by solids ($p < 0.05$), the k value in RUN X4 (k_{X4}, 7.02×10^{-1} h^{-1}) was almost the same as that in RUN X5 (k_{X5}, 4.92×10^{-1} h^{-1}) ($p > 0.05$). To quantitatively evaluate the effect of N_0 on *R. solanacearum* inactivation by each reactor, ratios of k values during 0–6 h (k_{X3}/k_{X2}, k_{X5}/k_{X4}) were calculated, and k_{X5}/k_{X4} was compared with k_{X3}/k_{X2}. k_{X5}/k_{X4} (7.01×10^{-1}) was around 9 times higher than k_{X3}/k_{X2} (7.82×10^{-2}), showing that the RAOC greatly improves the attenuation of UV intensity compared with the SSPR.

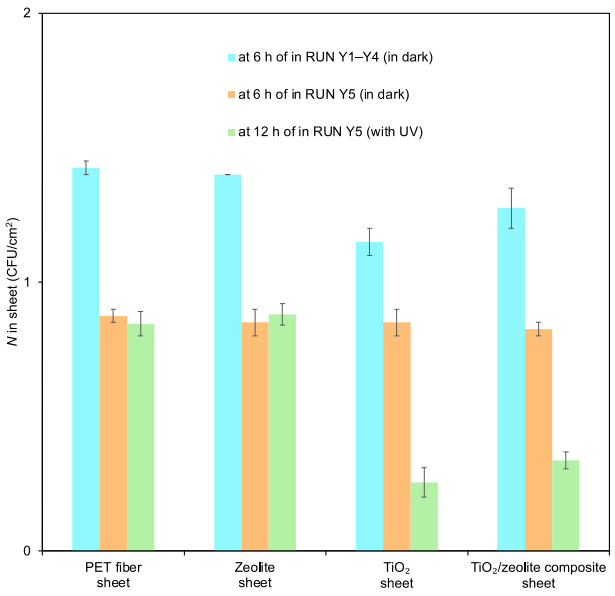

Fig. 4. The number of living bacteria (N) in each sheet. In RUNs Y1–Y4, the sheet was taken at 6 h. In RUN Y5, the sheet was taken at 6 h and 12 h. The plots are the average of measured values, and error bars denote the range of measures values ($n = 2$).

3.3. Deceleration of inactivation of *R. solanacearum* in PS during treatment

Behaviors of log (N/N_0) during 0–6 h were different from those during 6–24 h in RUNs X2, X4, and X5 (Fig. 2). Regression lines during 0–6 and 6–24 h were drawn (Fig. S2), and the k values in each time range in RUNs X2–X5 were determined from the slopes of the regression lines (Fig. 7a). In RUNs X2, X4, and X5, the k values during 6–24 h (1.33×10^{-1} h^{-1} in RUN X2, 9.64×10^{-2} h^{-1} in RUN X4, and 1.04×10^{-1} h^{-1} in RUN X5) were significantly lower than those during 0–6 h (4.09×10^{-1} h^{-1} in RUN X2, 7.02×10^{-1} h^{-1} in RUN X4, and 4.92×10^{-1} h^{-1} in RUN X5). In RUN X3, the k value during 6–24 h (4.98×10^{-2} h^{-1}) was almost same as that during 0–6 h (3.20×10^{-2} h^{-1}) because the *R. solanacearum* was hardly inactivated by the SSPR. Singh et al. (2016) applied a pulsed power technique to inactivate *Escherichia coli*, which is a Gram-negative bacterium, in water and investigated the inactivation mechanism of *E. coli* by the reactive oxygen species including hydroxyl radicals [57]. They found that inactivation of *E. coli* proceeds, in sequence, by formation of micropores caused by damage to the cell wall and cellular membrane, leakage from the cytoplasm, cell clumping, and accumulation of cell debris. They also mentioned that formation of micropores leads to release of proteins to the outside of the cell, and DNA inside the cell is damaged by the reactive oxygen species, resulting in the inactivation of *E. coli*. Benabbou et al. and Marugán et al. explored the kinetics of inactivation of *E. coli* by photocatalysis using TiO_2 and mentioned that the competition for reactive oxygen species between *E. coli* and the organic matter derived from inactivated *E. coli* is important for modeling [58–60]. *R. solanacearum* is also a Gram-negative bacterium, and the inactivation mechanism of *R. solanacearum* might be similar to that of *E. coli*. Organic matter containing aromatic moieties or peptide bonds (e.g., protein and phenol) absorbs light at 230 nm, while DNA exhibits weak absorption of light at 230 nm [61]; thus, the behavior of A_{230} was explored to monitor the release of organic matter from the cell if cell membranes were being damaged (Fig. 7b). A_{660} and A_{365} tended to decrease with the treatment (Fig. 6), but the behavior of A_{230} was totally different. In RUN X2, $A_{230}/A_{0,230}$ increased until 4 h and then decreased during 4–24 h. In RUN X3, $A_{230}/A_{0,230}$ tended to increase until 24 h. In RUN X4, $A_{230}/A_{0,230}$ decreased until 3 h and then became stable. In RUN X5, $A_{230}/A_{0,230}$ decreased until 2 h and then continuously increased until 24 h. The increase in A_{230} might be attributed to proteins released outside the cell and products derived from cell lysis. In previous studies, deactivation of TiO_2 by accumulation of organic compounds has been reported [62,63]. The deactivation of TiO_2 by accumulation of byproducts may be a reason for the deceleration of inactivation of *R. solanacearum*. We deduce that the inactivation of *R. solanacearum* decelerated after 6 h, possibly because of competition for reactive oxygen species between *R. solanacearum* and the products accumulated by inactivation of *R. solanacearum*.

3.4. Inhibitory effects of coexisting substances in the DS on inactivation of *R. solanacearum* by SSPR

In RUN X6, the inactivation efficiency of *R. solanacearum* in DS by the

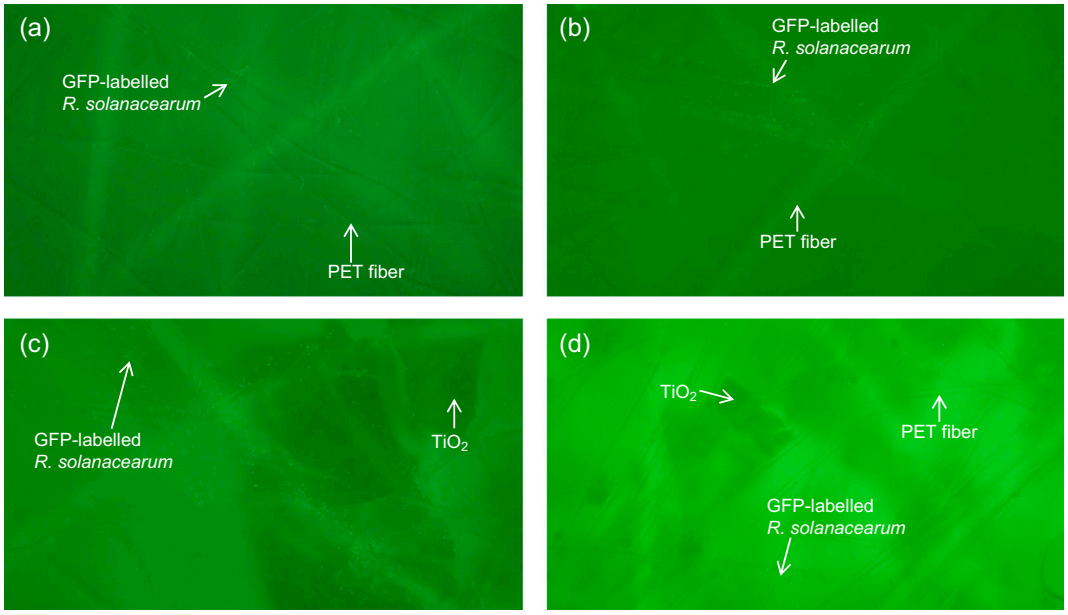

Fig. 5. The fluorescence images of PET fiber sheet (a, RUN Y1), zeolite sheet (b, RUN Y2), TiO_2 sheet (c, RUN Y3), and TiO_2/zeolite sheet (d, RUN Y4). RUNs Y1–Y4 were conducted in dark. Sheet samples were taken after 6 h of SSPR treatment, and the surface of sheet was observed using fluorescence microscope.

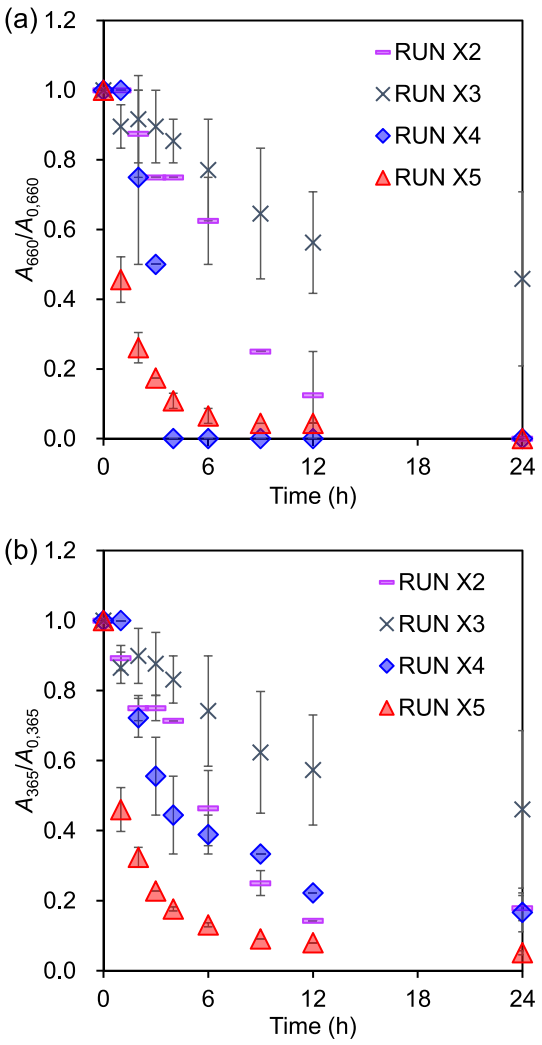

Fig. 6. Time profile of ratio of absorbance at 660 nm to the initial value (a, $A_{660}/A_{0,660}$) and 365 nm to the initial value (b, $A_{365}/A_{0,365}$). The SSPR was used in RUNs X2 and X3, and the RAOC was used in RUNs X4 and X5. The $A_{0,660}$ in RUNs X2, X3, X4, and X5 were 0.004, 0.023, 0.002, and 0.021, respectively. The $A_{0,365}$ in RUNs X2, X3, X4, and X5 were 0.013, 0.084, 0.009, and 0.088, respectively. In RUNs X2–X5, pure culture solution (PS) was used as solvent, and the water temperature was adjusted at 25 ± 1 °C. RUNs X2–X5 were performed with UV illumination of 1 mW cm^{-2}. The plots are the average of measured values, and error bars denote the range of measured values (n = 2).

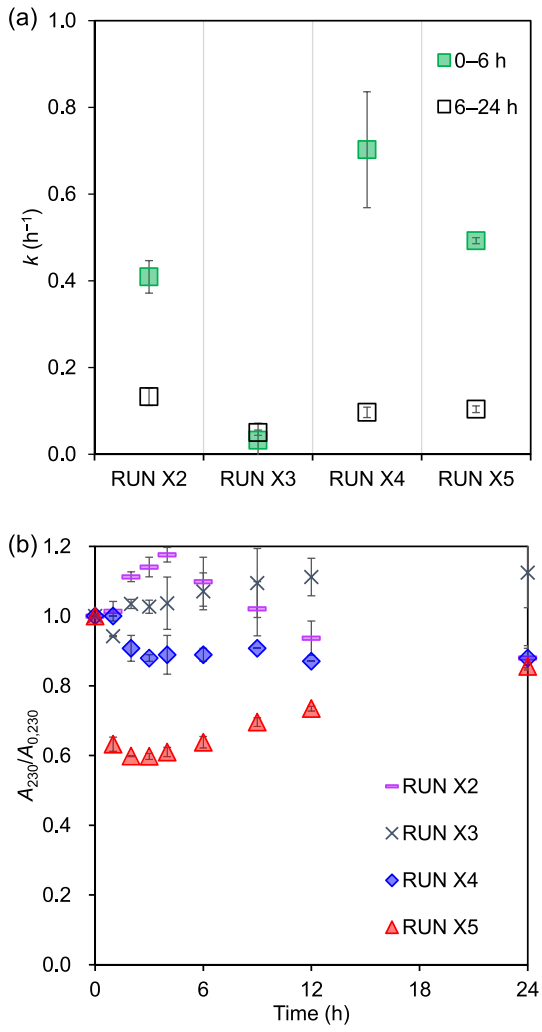

Fig. 7. Pseudo-first order rate constants (k) for inactivation of *R. solanacearum* during 0–6 and 6–24 h in RUNs X2–X5 (a), and time profile of the absorbance ratio at 230 nm to the initial value (b, $A_{230}/A_{0,230}$). The SSPR was used in RUNs X2 and X3, and the RAOC was used in RUNs X4 and X5. The $A_{0,230}$ in RUNs X2, X3, X4, and X5 were 0.076, 0.504, 0.055, and 0.498, respectively. In RUNs X2–X5, pure culture solution (PS) was used as solvent, and the water temperature was adjusted at 25 ± 1 °C. RUNs X2–X5 were performed with UV illumination of 1 mW cm^{-2}. The plots are the average of measured values, and error bars denote the range of measured values (n = 2).

SSPR was assessed (Fig. 8). Log (N/N_0) slightly decreased, and only 0.1-log reduction was observed during 6 h of SSPR treatment. The k value in RUN X6 (k_{X6}, 4.74 × 10^{-2} h^{-1}) was an order of magnitude lower than that in RUN X2 (k_{X2}, 4.09 × 10^{-1} h^{-1}), despite N_0 being nearly the same. This shows that coexisting substances in the DS strongly inhibited the inactivation of *R. solanacearum* ($p < 0.05$). The DS used in this study contains organics and inorganics at high concentration (Table 1). In hydroponic systems, organic matter is released from substrate and plant roots to the culture solution. Some organics absorb UV light and decrease the production of hydroxyl radicals and holes (h^+) [64–66]. Anions such as HCO_3^-/CO_3^{2-} scavenge hydroxyl radicals and are strong inhibitors of photocatalysis of target compounds [67]. Therefore, the SSPR is not an applicable reactor for the inactivation of *R. solanacearum* in DS, and development of a reactor that mitigates the light attenuation and inhibitory effects of coexisting substances is essential.

3.5. Mitigation of inhibitory effects of coexisting substances in the DS on *R. solanacearum* inactivation by the RAOC

In RUN X7, the inactivation efficiency of *R. solanacearum* in DS by using the RAOC was investigated, and >2-log inactivation was achieved during 24 h of RAOC treatment (Fig. 8). The k value during 0–6 h in RUN X7 (k_{X7}, 6.44 × 10^{-1} h^{-1}) was nearly same as that in RUN X4 (k_{X4}, 7.02 × 10^{-1} h^{-1}), showing that the RAOC mitigates the inhibitory effects of coexisting substances in the DS on inactivation of *R. solanacearum* ($p > 0.05$). The SSPR could not inactivate *R. solanacearum* in the DS because of strong inhibition by coexisting substances. In contrast, the RAOC showed excellent performance in inactivation of *R. solanacearum*. For quantitative evaluation of the mitigation of inhibition, the ratio of k values in PS and DS by each reactor (k_{X6}/k_{X2}, k_{X7}/k_{X4}) was determined. k_{X7}/k_{X4} (9.17 × 10^{-1}) was nearly 8 times k_{X6}/k_{X2} (1.16 × 10^{-1}), demonstrating that the RAOC strongly mitigates the inhibitory effects of coexisting substances in the DS on inactivation of *R. solanacearum*. In the RAOC, the attenuation of UV intensity by water was negligible. We previously found that a RAOC effectively removed 1,4-dioxane from

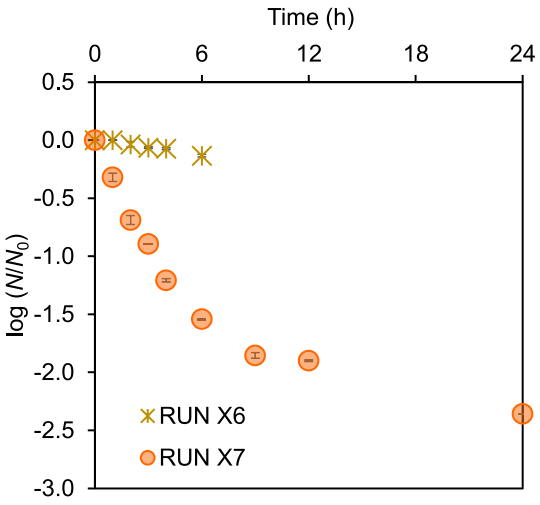

Fig. 8. Inactivation of *R. solanacearum* in drainage solution (DS) by the SSPR (RUN X6) and RAOC (RUN X7). The SSPR was used in RUN X6, and the RAOC was used in RUN X7. In RUNs X6 and X7, the water temperature was adjusted at 25 ± 1 °C. RUNs X6 and X7 were performed with UV illumination of 1 mW cm^{-2}. The plots are the average of measured values, and error bars denote the range of measured values ($n = 2$).

landfill leachate containing coexisting substances at high concentration, and discussed the mechanism of mitigation of the inhibitory effects of the coexisting substances [40]. In the RAOC, the attenuation of UV intensity is negligible because the average thickness of the water film that is formed on the disk is only 1.3×10^2 μm, and the very thin water film contributed to efficient removal of 1,4-dioxane from landfill leachate [40]. The mechanism of mitigation of the inhibition of *R. solanacearum* inactivation might be similar to that reported in our previous study. Corona plasma-based inactivation technology for *R. solanacearum* has been reported [19–21,23], but previous studies have not determined the inactivation efficiency of *R. solanacearum* in actual DS. In addition, the corona plasma reactor cannot easily be scaled-up because the corona plasma is generated in a very narrow cylinder under high voltage and continuous air flow. The RAOC showed excellent performance in the inactivation of *R. solanacearum* in the DS under irradiation by UVA light, which is abundant in sunlight, and thus this will be an energy-saving reactor for the disinfection of DS containing *R. solanacearum*. The RAOC is therefore a promising and upscalable photocatalytic reactor for efficiently inactivating *R. solanacearum* in DS.

4. Conclusions

In this study, an RAOC equipped with TiO_2/zeolite composite sheets was developed to inactivate *R. solanacearum* in DS. The inactivation efficiency of *R. solanacearum* in the DS by the RAOC was evaluated by comparing with that by a SSPR. Inhibitory effects of coexisting substances in the DS on the inactivation of *R. solanacearum* were investigated. The mechanism of mitigation of the inhibition was also assessed. The main findings are:

- The SSPR inactivated *R. solanacearum* in the PS through photocatalysis by the TiO_2/zeolite composite sheet, but the inactivation efficiency at 4.0×10^7 CFU mL^{-1} of N_0 significantly decreased compared with that at 1.8×10^6 CFU mL^{-1} of N_0 owing to the attenuation of UV intensity by light absorption and scattering by solids derived from *R. solanacearum*. The GFP-labelled *R. solanacearum* was mainly observed on PET fibers in the TiO_2/zeolite composite sheet.
- The RAOC achieved >2-log inactivation during 24 h of treatment regardless of N_0. *R. solanacearum* captured by the sheet was inactivated through photocatalysis by the TiO_2/zeolite composite sheet under UV irradiation. k_{X5}/k_{X4} was around 9 times higher than k_{X3}/k_{X2}. This shows that the RAOC greatly improves the attenuation of UV intensity compared with the SSPR.
- A deceleration of inactivation of *R. solanacearum* and an increase in A_{230} were observed in RUNs X2–X5. The increase in A_{230} might be attributed to proteins released outside the cell and products derived from cell lysis. We deduce that the inactivation of *R. solanacearum* decelerated after 6 h, possibly because of competition for reactive oxygen species between living *R. solanacearum* and the products accumulated by inactivation of *R. solanacearum*.
- Coexisting substances in the DS strongly inhibited the inactivation of *R. solanacearum* by the SSPR; only 0.1-log reduction was observed during 6 h of SSPR treatment. In contrast, the RAOC showed excellent performance in inactivation of *R. solanacearum* in the DS, and > 2-log inactivation was achieved during 24 h of RAOC treatment. k_{X7} was nearly the same as k_{X4}, and k_{X7}/k_{X4} was nearly 8 times k_{X6}/k_{X2}, showing that the RAOC mitigates the light attenuation and inhibitory effects of coexisting substances on inactivation of *R. solanacearum* in the DS. This might be because of the very thin water film used by the RAOC.
- The RAOC is a promising and upscalable photocatalytic reactor for efficiently inactivating *R. solanacearum* in DS.

Declaration of competing interest

The authors declare that they have no known competing financial interests or personal relationships that could have appeared to influence the work reported in this paper.

Acknowledgements

This work was supported by Cabinet Office grant-in-aid, the Advanced Next-Generation Greenhouse Horticulture by IoP (Internet of Plants), Japan. This research was supported by JSPS KAKENHI grant-numbers JP20K06054 and JP17K07667. We thank James Allen, DPhil, from Edanz Group (https://en-author-services.edanzgroup.com/ac) for editing a draft of this manuscript.

Appendix A. Supplementary data

Supplementary data to this article can be found online at https://doi.org/10.1016/j.jwpe.2022.102936.

References

[1] United Nations, World Population Prospects 2019, 2019.
[2] World Resources Institute, Creating a Sustainable Food Future, 2019.
[3] M. Albaho, B. Thomas, A. Christopher, Evaluation of hydroponic techniques on growth and productivity of greenhouse grown bell pepper and strawberry, Int. J. Veg. Sci. 14 (2008) 23–40, https://doi.org/10.1080/19315260801890492.
[4] V. Valenzano, A. Parente, F. Serio, P. Santamaria, Effect of growing system and cultivar on yield and water-use efficiency of greenhouse-grown tomato, J. Hortic. Sci. Biotechnol. 83 (2008) 71–75, https://doi.org/10.1080/14620316.2008.11512349.
[5] K. Kondo, K. Inoue, T. Fujiwara, S. Yamane, D. Yasutake, M. Maeda, H. Nagare, S. Akao, K. Ohtoshi, Seasonal changes in the performance of a catch crop for mitigating diffuse agricultural pollution, Water Sci. Technol. 68 (2013) 776–782, https://doi.org/10.2166/wst.2013.258.
[6] S. Hashida, M. Johkan, K. Kitazaki, K. Shoji, F. Goto, T. Yoshihara, Management of nitrogen fertilizer application, rather than functional gene abundance, governs nitrous oxide fluxes in hydroponics with rockwool, Plant Soil 374 (2014) 715–725, https://doi.org/10.1007/s11104-013-1917-4.
[7] S. Koike, K. Subbarao, R.M. Davis, T. Turini, Vegetable Diseases Caused by Soilborne Pathogens, UCANR Publications, 2003, https://doi.org/10.3733/ucanr.8099.
[8] E.R. Graber, O. Frenkel, A.K. Jaiswal, Y. Elad, How may biochar influence severity of diseases caused by soilborne pathogens? Carbon Manag. 5 (2014) 169–183, https://doi.org/10.1080/17583004.2014.913360.
[9] S. Hosseinzadeh, Y. Verheust, G. Bonarrigo, S. Van Hulle, Closed hydroponic systems: operational parameters, root exudates occurrence and related water

treatment, Rev. Environ. Sci. Biotechnol. 16 (2017) 59–79, https://doi.org/10.1007/s11157-016-9418-6.
[10] F.A. Khan, A. Kurklu, A. Ghafoor, Q. Ali, M. Umair, Shahzaib, A review on hydroponic greenhouse cultivation for sustainable agriculture, Int. J. Agric. Environ. Food Sci. 2 (2018) 59–66, https://doi.org/10.31015/jaefs.18031.
[11] N. Sharma, S. Acharya, K. Kumar, N. Singh, O.P. Chaurasia, Hydroponics as an advanced technique for vegetable production: an overview, J. Soil Water Conserv. 17 (2018) 364, https://doi.org/10.5958/2455-7145.2018.00056.5.
[12] K.-W. Nam, B.-W. Moon, Y.-H. Kim, C.-H. Lee, Infection route of bacterial wilt of tomato caused by ralstonia solanacearum in hydroponic culture, J. Bio-Environ. Control 18 (2009) 171–176.
[13] W. Runia, E. Van Os, G. Bollen, Disinfection of drainwater from soillness cultures by heat treatment, Netherlands, J. Agric. Sci. 36 (1988) 231–238, https://doi.org/10.18174/njas.v36i3.16674.
[14] A.C. Schuerger, W. Hammer, Use of cross-flow membrane filtration in a recirculating hydroponic system to suppress root disease in pepper caused by *Pythium myriotylum*, Phytopathology 99 (2009) 597–607, https://doi.org/10.1094/PHYTO-99-5-0597.
[15] J. Mori, R. Smith, Transmission of waterborne fish and plant pathogens in aquaponics and their control with physical disinfection and filtration: a systematized review, Aquaculture 504 (2019) 380–395, https://doi.org/10.1016/j.aquaculture.2019.02.009.
[16] D.L. Ehret, B. Alsanius, W. Wohanka, J.G. Menzies, R. Utkhede, Disinfestation of recirculating nutrient solutions in greenhouse horticulture, Agronomie 21 (2001) 323–339, https://doi.org/10.1051/agro:2001127.
[17] J.E. Holland, A.E. Bennett, A.C. Newton, P.J. White, B.M. McKenzie, T.S. George, R.J. Pakeman, J.S. Bailey, D.A. Fornara, R.C. Hayes, Liming impacts on soils, crops and biodiversity in the UK: a review, Sci. Total Environ. 610–611 (2018) 316–332, https://doi.org/10.1016/j.scitotenv.2017.08.020.
[18] M.H. Kang, A. Pengkit, K. Choi, S.S. Jeon, H.W. Choi, D.B. Shin, E.H. Choi, H. S. Uhm, G. Park, Differential inactivation of fungal spores in water and on seeds by ozone and arc discharge plasma, PLoS One 10 (2015) 1–16, https://doi.org/10.1371/journal.pone.0139263.
[19] S.-E. Back, D.-S. Kim, Y.-S. Park, Inactivation of *Ralstonia solanacearum* using aquatic plasma process, J. Environ. Sci. Int. 21 (2012) 797–804, https://doi.org/10.5322/jes.2012.21.7.797.
[20] D.-S. Kim, Y.-S. Park, A study on the *Ralstonia solanacearum* inactivation using improved plasma process, J. Environ. Sci. Int. 23 (2014) 369–378, https://doi.org/10.5322/jesi.2014.23.3.369.
[21] T. Okumura, Y. Saito, K. Takano, K. Takahashi, K. Takaki, N. Satta, T. Fujio, Inactivation of bacteria using discharge plasma under liquid fertilizer in a hydroponic culture system, Plasma Med. 6 (2016) 247–254, https://doi.org/10.1615/PlasmaMed.2016018683.
[22] Y. Park, Inactivation of wilt germs (*Fusarium oxysporum f. sp. radicis lycopersici*) using dielectric barrier discharge plasma in hydroponic cultivation system, J. Environ. Sci. Int. 28 (2019) 495–502.
[23] K. Takahashi, Y. Saito, R. Oikawa, T. Okumura, K. Takaki, T. Fujio, Development of automatically controlled corona plasma system for inactivation of pathogen in hydroponic cultivation medium of tomato, J. Electrost. 91 (2018) 61–69, https://doi.org/10.1016/j.elstat.2017.12.006.
[24] W. Zhang, J.C. Tu, Effect of ultraviolet disinfection of hydroponic solutions on pythium root rot and non-target bacteria, Eur. J. Plant Pathol. 106 (2000) 415–421, https://doi.org/10.1023/A:1008798710325.
[25] C. Sichel, M. de Cara, J. Tello, J. Blanco, P. Fernández-Ibáñez, Solar photocatalytic disinfection of agricultural pathogenic fungi: *Fusarium* species, Appl. Catal. B Environ. 74 (2007) 152–160, https://doi.org/10.1016/j.apcatb.2007.02.005.
[26] S.W. Chung, Y.S. Ha, K.Y. Lee, J.S. Kim, J.M. Park, S.G. Kwon, W.S. Choi, S. H. Kwon, M. Mitusoka, E. Inoue, T. Okayasu, Sterilization in hydroponic recycling system using visible light-reactive titanium dioxide photocatalysts, J. Fac. Agric. Kyushu Univ. 58 (2013) 93–98, https://doi.org/10.5109/26166.
[27] S. Date, T. Hataya, T. Namiki, Effects of nutrient and environmental pre-treatments on the occurrence of root injury of lettuce cause by shloramine, Acta Hortic. 481 (1999) 553–560. https://doi.org/10.17660/ActaHortic.1999.481.65.
[28] B.A. Younis, L. Mahoney, W. Schweigkofler, K. Suslow, Inactivation of plant pathogens in irrigation water runoff using a novel UV disinfection system, Eur. J. Plant Pathol. 153 (2019) 907–914, https://doi.org/10.1007/s10658-018-01608-8.
[29] T. Koutchma, S. Keller, S. Chirtel, B. Parisi, Ultraviolet disinfection of juice products in laminar and turbulent flow reactors, Innov. Food Sci. Emerg. Technol. 5 (2004) 179–189, https://doi.org/10.1016/j.ifset.2004.01.004.
[30] K. Fujiwara, C. Aoyama, M. Takano, M. Shinohara, Suppression of *Ralstonia solanacearum* bacterial wilt disease by an organic hydroponic system, J. Gen. Plant Pathol. 78 (2012) 217–220, https://doi.org/10.1007/s10327-012-0371-0.
[31] M.A. Schell, Control of virulence and pathogenicity genes of *Ralstonia solanacearum* by an elaborate sensory network, Annu. Rev. Phytopathol. 38 (2000) 263–292, https://doi.org/10.1146/annurev.phyto.38.1.263.
[32] Y. Hikichi, Y. Mori, S. Ishikawa, K. Hayashi, K. Ohnishi, A. Kiba, K. Kai, Regulation involved in colonization of intercellular spaces of host plants in *Ralstonia solanacearum*, Front. Plant Sci. 8 (2017) 1–6, https://doi.org/10.3389/fpls.2017.00967.
[33] H. Nagare, Y. Nomura, K. Nakanishi, S. Akao, T. Fujiwara, Characterization of effluent water quality from hydroponic cultivation system, J. Water Environ. Technol. 19 (2021) 64–73, https://doi.org/10.2965/jwet.20-096.
[34] G.V. Buxton, C.L. Greenstock, W.P. Helman, A.B. Ross, Critical review of rate constants for reactions of hydrated electrons, hydrogen atoms and hydroxyl radicals (·OH/·O$^-$ in aqueous solution, J. Phys. Chem. Ref. Data 17 (1988) 513–886, https://doi.org/10.1063/1.555805.
[35] D. Minakata, K. Li, P. Westerhoff, J. Crittenden, Development of a group contribution method to predict aqueous phase hydroxyl radical (HO·) reaction rate constants, Environ. Sci. Technol. 43 (2009) 6220–6227, https://doi.org/10.1021/es900956c.
[36] Q. Xiang, S. Fukahori, N. Yamashita, H. Tanaka, T. Fujiwara, Removal of crotamiton from reverse osmosis concentrate by a TiO_2/zeolite composite sheet, Appl. Sci. 7 (2017) 778, https://doi.org/10.3390/app7080778.
[37] S. Fukahori, T. Fujiwara, Preparation of flexible TiO_2/zeolite composite sheets for removal of sulfamethazine from wastewater using papermaking technique, J. Water Environ. Technol. 17 (2019) 395–406, https://doi.org/10.2965/jwet.19-030.
[38] S. Fukahori, T. Fujiwara, R. Ito, N. Funamizu, Sulfonamide antibiotic removal and nitrogen recovery from synthetic urine by the combination of rotating advanced oxidation contactor and methylene urea synthesis process, Water Sci. Technol. 72 (2015) 238, https://doi.org/10.2166/wst.2015.182.
[39] S. Fukahori, M. Ito, T. Fujiwara, Removal mechanism of sulfamethazine and its intermediates from water by a rotating advanced oxidation contactor equipped with TiO_2–high-silica zeolite composite sheets, Environ. Sci. Pollut. Res. 25 (2018) 29017–29025, https://doi.org/10.1007/s11356-018-2909-y.
[40] Y. Nomura, S. Fukahori, T. Fujiwara, Removal of 1,4-dioxane from landfill leachate by a rotating advanced oxidation contactor equipped with activated carbon/TiO_2 composite sheets, J. Hazard. Mater. 383 (2020), 121005, https://doi.org/10.1016/j.jhazmat.2019.121005.
[41] Y. Nomura, S. Fukahori, T. Fujiwara, Removal of sulfamonomethoxine and its transformation byproducts from fresh aquaculture wastewater by a rotating advanced oxidation contactor equipped with zeolite/TiO_2 composite sheets, Process Saf. Environ. Prot. 134 (2020) 161–168, https://doi.org/10.1016/j.psep.2019.11.036.
[42] Y. Nomura, S. Fukahori, T. Fujiwara, Thermodynamics of removing crotamiton and its transformation byproducts from water by a rotating advanced oxidation contactor with zeolite/TiO_2 composite sheets, Chem. Eng. J. 380 (2020), 122479, https://doi.org/10.1016/j.cej.2019.122479.
[43] Q. Xiang, Y. Nomura, S. Fukahori, T. Mizuno, H. Tanaka, T. Fujiwara, Innovative treatment of organic contaminants in reverse osmosis concentrate from water reuse: a mini review, Curr. Pollut. Rep. 5 (2019) 294–307, https://doi.org/10.1007/s40726-019-00119-2.
[44] Q. Xiang, S. Fukahori, N. Yamashita, H. Tanaka, T. Fujiwara, Removing crotamiton from reverse osmosis concentrate by using coagulation and a rotating advanced oxidation contactor, Environ. Qual. Manag. (2020) 1–10, https://doi.org/10.1002/tqem.21714.
[45] A. Kanda, S. Ohnishi, H. Tomiyama, H. Hasegawa, M. Yasukohchi, A. Kiba, K. Ohnishi, T. Okuno, Y. Hikichi, Type III secretion machinery-deficient mutants of *Ralstonia solanacearum* lose their ability to colonize resulting in loss of pathogenicity, J. Gen. Plant Pathol. 69 (2003) 250–257, https://doi.org/10.1007/s10327-003-0041-3.
[46] C.A. Boucher, P.A. Barberis, A.P. Trigalet, D.A. Demery, Transposon mutagenesis of *Pseudomonas solanacearum*: isolation of Tn5-induced avirulent mutants, Microbiology 131 (1985) 2449–2457, https://doi.org/10.1099/00221287-131-9-2449.
[47] Y. Mori, K. Inoue, K. Ikeda, H. Nakayashiki, C. Higashimoto, K. Ohnishi, A. Kiba, Y. Hikichi, The vascular plant-pathogenic bacterium *Ralstonia solanacearum* produces biofilms required for its virulence on the surfaces of tomato cells adjacent to intercellular spaces, Mol. Plant Pathol. 17 (2016) 890–902, https://doi.org/10.1111/mpp.12335.
[48] J.L. Ruiz-Barba, A. Maldonado, R. Jiménez-Díaz, Small-scale total DNA extraction from bacteria and yeast for PCR applications, Anal. Biochem. 347 (2005) 333–335, https://doi.org/10.1016/j.ab.2005.09.028.
[49] J.G. Elphinstone, J. Hennessy, J.K. Wilson, D.E. Stead, Sensitivity of different methods for the detection of *Ralstonia solanacearum* in potato tuber extracts, Bull. OEPP/EPPO Bull. 26 (1996) 663–678, https://doi.org/10.1111/j.1365-2338.1996.tb01511.x.
[50] L. Chen, M. Shirota, Y. Zhang, A. Kiba, Y. Hikichi, K. Ohnishi, Involvement of HLK effectors in *Ralstonia solanacearum* disease development in tomato, J. Gen. Plant Pathol. 80 (2014) 79–84, https://doi.org/10.1007/s10327-013-0490-2.
[51] H. Chick, An investigation of the laws of disinfection, J. Hyg. (Lond) 8 (1908) 92–158, https://doi.org/10.1017/S0022172400006987.
[52] H.E. Watson, A note on the variation of the rate of disinfection with change in the concentration of the disinfectant, Epidemiol. Infect. 8 (1908) 536–542, https://doi.org/10.1017/S0022172400015928.
[53] Y. Shimizu, M. Ateia, M. Wang, D. Awfa, C. Yoshimura, Disinfection mechanism of *E. coli* by CNT-TiO_2 composites: photocatalytic inactivation vs. Physical separation, Chemosphere 235 (2019) 1041–1049, https://doi.org/10.1016/j.chemosphere.2019.07.006.
[54] M. Ateia, M.G. Alalm, D. Awfa, M.S. Johnson, C. Yoshimura, Modeling the degradation and disinfection of water pollutants by photocatalysts and composites: a critical review, Sci. Total Environ. 698 (2020), 134197, https://doi.org/10.1016/j.scitotenv.2019.134197.
[55] K.C. Lee, K.H. Choo, Hybridization of TiO_2 photocatalysis with coagulation and flocculation for 1,4-dioxane removal in drinking water treatment, Chem. Eng. J. 231 (2013) 227–235, https://doi.org/10.1016/j.cej.2013.07.023.
[56] R.J. Wu, C.C. Chen, M.H. Chen, C.S. Lu, Titanium dioxide-mediated heterogeneous photocatalytic degradation of terbufos: parameter study and reaction pathways, J. Hazard. Mater. 162 (2009) 945–953, https://doi.org/10.1016/j.jhazmat.2008.05.121.

[57] R.K. Singh, L. Philip, S. Ramanujam, Disinfection of water by pulsed power technique: a mechanistic perspective, RSC Adv. 6 (2016) 11980–11990, https://doi.org/10.1039/c5ra26941e.
[58] A.K. Benabbou, Z. Derriche, C. Felix, P. Lejeune, C. Guillard, Photocatalytic inactivation of *Escherischia coli*: effect of concentration of TiO_2 and microorganism, nature, and intensity of UV irradiation, Appl. Catal. B Environ. 76 (2007) 257–263, https://doi.org/10.1016/j.apcatb.2007.05.026.
[59] J. Marugán, R. van Grieken, C. Sordo, C. Cruz, Kinetics of the photocatalytic disinfection of *Escherichia coli* suspensions, Appl. Catal. B Environ. 82 (2008) 27–36, https://doi.org/10.1016/j.apcatb.2008.01.002.
[60] J. Marugán, R. van Grieken, C. Pablos, M.L. Satuf, A.E. Cassano, O.M. Alfano, Rigorous kinetic modelling with explicit radiation absorption effects of the photocatalytic inactivation of bacteria in water using suspended titanium dioxide, Appl. Catal. B Environ. 102 (2011) 404–416, https://doi.org/10.1016/j.apcatb.2010.12.012.
[61] S.R. Gallagher, Quantitation of DNA and RNA with absorption and fluorescence spectroscopy, Curr. Protoc. Immunol. 2017 (2017), https://doi.org/10.1002/cpim.20. A.3L.1-A.3L.14.
[62] R. Méndez-Román, N. Cardona-Martínez, Relationship between the formation of surface species and catalyst deactivation during the gas-phase photocatalytic oxidation of toluene, Catal. Today. 40 (1998) 353–365, https://doi.org/10.1016/S0920-5861(98)00064-9.
[63] L. Cao, Z. Gao, S.L. Suib, T.N. Obee, S.O. Hay, J.D. Freihaut, Photocatalytic oxidation of toluene on nanoscale TiO_2 catalysts: studies of deactivation and regeneration, J. Catal. 196 (2000) 253–261, https://doi.org/10.1006/jcat.2000.3050.
[64] C. Jia, Y. Wang, C. Zhang, Q. Qin, UV-TiO_2 photocatalytic degradation of landfill leachate, Water Air Soil Pollut. 217 (2011) 375–385, https://doi.org/10.1007/s11270-010-0594-7.
[65] M. Antonopoulou, V. Papadopoulos, I. Konstantinou, Photocatalytic oxidation of treated municipal wastewaters for the removal of phenolic compounds: optimization and modeling using response surface methodology (RSM) and artificial neural networks (ANNs), J. Chem. Technol. Biotechnol. 87 (2012) 1385–1395, https://doi.org/10.1002/jctb.3755.
[66] W.H.M. Abdelraheem, X. He, X. Duan, D.D. Dionysiou, Degradation and mineralization of organic UV absorber compound 2-phenylbenzimidazole-5-sulfonic acid (PBSA) using UV-254nm/H_2O_2, J. Hazard. Mater. 282 (2015) 233–240, https://doi.org/10.1016/j.jhazmat.2014.07.041.
[67] J. Wiszniowski, D. Robert, J. Surmacz-Gorska, K. Miksch, S. Malato, J.V. Weber, Solar photocatalytic degradation of humic acids as a model of organic compounds of landfill leachate in pilot-plant experiments: influence of inorganic salts, Appl. Catal. B Environ. 53 (2004) 127–137, https://doi.org/10.1016/j.apcatb.2004.04.017.